Hydrodynamics and heat transfer during flow boiling instabilities in a single microchannel

Jacqueline Barber, Khellil Sefiane, David Brutin, Lounes Tadrist

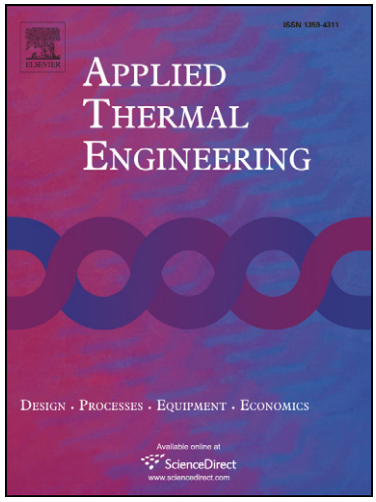

Hydrodynamics and heat transfer during flow boiling instabilities in a single microchannel

Jacqueline Barber, Khellil Sefiane, David Brutin, Lounes Tadrist

PII: S1359-4311(08)00302-5
DOI: 10.1016/j.applthermaleng.2008.07.004
Reference: ATE 2565

To appear in: *Applied Thermal Engineering*

Received Date: 14 December 2007
Revised Date: 2 July 2008
Accepted Date: 4 July 2008

Please cite this article as: J. Barber, K. Sefiane, D. Brutin, L. Tadrist, Hydrodynamics and heat transfer during flow boiling instabilities in a single microchannel, *Applied Thermal Engineering* (2008), doi: 10.1016/j.applthermaleng.2008.07.004

HYDRODYNAMICS AND HEAT TRANSFER DURING FLOW BOILING INSTABILITIES IN A SINGLE MICROCHANNEL

Jacqueline Barber[1, 2*], Khellil Sefiane[1], David Brutin[2] and Lounes Tadrist[2]

[1]School of Engineering and Electronics, University of Edinburgh, Scotland, EH9 3JL, Fax No: +44131650 6551

[2]Département de Mécanique Energétique, Polytechnique de Marseille, France, 13453

* (author correspondent: J.Barber@ed.ac.uk, Tel. No: +441316505691)

ABSTRACT

Boiling in microchannels is widely considered as one of the front runners in process intensification heat removal. Flow boiling heat transfer in microchannel geometry and the associated flow instabilities are not well understood, further research is necessary into the flow instabilities adverse effect on heat transfer.

Boiling is induced in microchannel geometry (hydraulic diameter 727 μm) to investigate several flow instabilities. A transparent, metallic, conductive deposit has been developed on the exterior of rectangular microchannels, allowing simultaneous heating and visualisation.

Presented in this paper is data for a particular case with a uniform heat flux of 4.26 kW/m^2 applied to the microchannel and inlet liquid mass flowrate, held constant at $1.13x10^{-5}$ kg/s. In conjunction with obtaining high-speed images, a sensitive Infra Red camera is used to record the temperature profiles on the exterior wall of the microchannel, and a data acquisition system is used to record the pressure fluctuations over time. Various phenomena are apparent during the flow instabilities; these can be characterised into timescales occurring at 100's seconds, 10's seconds, several seconds and finally

milliseconds. Correlation of pressure oscillations with temperature fluctuations as a function of the heat flux applied to the microchannel is possible.

From analysis of our results, images and video sequences with the corresponding physical data obtained, it is possible to follow simultaneously particular flow, pressure and temperature conditions leading to nucleate boiling, flow instabilities and transition regimes during flow boiling in a microchannel. The investigation allowed us to quantify and characterise the timescales of various observed instabilities during flow boiling in a microchannel. High speed imaging revealed some of the controlling physical mechanisms responsible for the observed instabilities.

KEYWORDS: Boiling, microchannels, visualisation, flow instabilities.

1. INTRODUCTION

Boiling heat transfer can be applied to heat exchange processes and energy conversion. High heat and mass transfer coefficients are associated with single-phase flow and flow boiling in narrow channels. This has already made microchannels attractive in electronics cooling applications [1, 2], developments in Microelectromechanical systems (MEMS) devices, in the design of compact evaporators and heat exchangers [3, 4], inkjet printers and for process intensification, such as in space laboratories. Boiling flows are particularly important; they provide an effective method of fluid movement, less pumping power is required than single-phase liquid flow to achieve a given heat removal, and they have large heat dissipation capabilities. Microchannels can be used as micro-cooling elements for laptop computer chips, electronic components and aerospace avionics components; in these situations their compact size and heat transfer abilities are unrivalled.

The heat transfer process and hydrodynamics occurring in microchannels are distinctly different than that in macroscale flows [3, 5-7], so only some of the available macroscale knowledge can be applied to the microscale. Currently there is poor understanding of the mechanism of flow boiling heat transfer in microchannel geometry [8]. It was previously concluded by researchers that nucleate boiling controls evaporation in microchannels [9]. However, now it is thought that the controlling heat transfer mechanism is the evaporation of the thin liquid film around the bubbles inside microchannels [10]. There are several general literature reviews on the subject [11-13].

The modelling of the thin liquid film region and the meniscus region of capillary flows can be found in the literature [14-17]. The mechanisms concerning the development and the progression of a liquid-vapour interface through a microchannel are still unclear. Physical phenomena such as bubble confinement [3] and thin film evaporation have been recorded

by researchers, and subsequently attempts have been made to explain these observations. It is thought that surface tension, capillary forces and wall effects are dominant in small diameter channels. Various phenomena are observed as the bubble diameter approaches the channel diameter; that is as the bubbles become more confined. The channel's diameter can become so confining that only one bubble exists in the cross-section, sometimes becoming elongated. This is in stark contrast to flows seen in macrochannels, where numerous bubbles can exist at one time.

There are various flow instabilities noted in the literature [18-20] including temperature excursions, flow excursions, pressure fluctuations, channel dry-out and even reverse flow (possibly triggered by vapour recoil) in microchannels. It is of interest to further comprehend these instabilities. However two-phase and boiling flow instabilities are complex, due to phase change and the presence of several interfaces. To fully understand the high heat transfer potential of boiling flows in microchannels, it is vital to first understand the interline phenomena and how to model the evaporating meniscus in such a channel, as well as understanding the occurrence of the flow instabilities.

There are references in the literature to reverse flow [18, 21]. Flow visualisation was made with a high speed camera by Brutin et al. [18]. The flowing liquid enters the microchannel and nucleation begins. The wall superheat allows the vapour bubble produced to grow rapidly, coalescing and forming a vapour slug. Several investigators [17] have considered this vapour slug as an elongated bubble. This rapid bubble growth is greater than the rate the vapour can exit the channel. There is hence a vapour build-up in the channel, with a thin liquid film at the channel walls. Channel dry-out can occur and the over-pressure produced by the vapour slugs reduces the upstream boiling flowrate. Bubbles growing before the vapour slug slow down, and quickly the whole channel cross-section is filled. The vapour needs to expand, and the liquid-vapour interface at both sides of the vapour slug is pushed upstream and downstream. This leads to the inflowing liquid

being pushed back to the channel entrance, i.e. the vapour bubbles recoil, creating a reverse flow in the microchannel. It has been also noted by Brutin et al. [18] that pressure oscillations accompany the (afore mentioned) visual observations of flow reversal in a microchannel.

Surface temperature rises are expected to occur at equivalent times to the channel filling with vapour. Since the heat flux at the channel walls is usually removed by the fluid boiling, the surface temperature of the vapour-filled channel will rise dramatically. It is also thought that there will be hot spots of temperature at the triple point (bubble edges). Fluctuations in the pressure drop across the channel accompany the occurrence of flow reversal, with flow accelerations to refill the vapour spaces. When the channel is empty, and the pressure drop across the channel has been re-established, the liquid will once again begin to flow into the channel. Bubbles will be formed again quickly, due to the increased surface temperature of the channel, and the phenomena will be repeated. Physical quantities such as flowrate and pressure drop, as well as temperature variations, will be important variables in understanding and predicting the flow instability. It has been demonstrated by many authors [22-24] that during intense evaporation and high temperatures, vapour recoil instability can develop. The exact role and contribution of this mechanism is still not fully elucidated.

The differential vapour recoil mechanism was first noted by Hickman in 1952 [25] during his experiments on the evaporation of liquids at reduced pressures. A rapidly evaporating liquid in a confined space is not able to remain stable during local variations in the evaporation rate, i.e. the forces exerted at the interface when the vapour rapidly departs in conjunction with the sustaining liquid flows. This same situation can be found during flow boiling in a microchannel.

Several references in this paper are made to boiling experiments in a single microchannel. It is also important to note that there are many similar experiments

conducted on multiple, parallel microchannels too. These papers are also of importance and relevance, and a few of these works follow. In the literature there have been several researchers that use non-uniform heating in their microchannel research, i.e. with one face of their channels transparent for visualisation purposes. Peng and Wang [5] provided heating to a rectangular microchannel of cross section 600 x 700 μm, via three sides of the channel which had been micro-machined into a steel plate. Xu et al. [26] used a platinum film on the back of a silicon wafer to provide heating to ten parallel, triangular silicon microchannels of hydraulic diameter 155 μm. Zhang et al. [27] again used a heater adhered to the back face of a micro-machined silicon wafer, with rectangular microchannels of hydraulic diameter range 27-171 μm. Piasecka et al. [28] used a rectangular microchannel in which only one channel wall was heated uniformly, all other walls were approximately adiabatic. Qu and Mudawar [29] conducted saturated flow boiling experiments on a 21 parallel, rectangular (cross section 231 x 713 μm) microchannel heat sink, etched onto a silicon chip and with a heater adhered to the back face. Kenning et al. [30] had a single rectangular minichannel of cross section 2 x 1 mm, heated on three sides, with the fourth side used as a flow visualisation window. Brutin and Tadrist [31] used a single rectangular minichannel, of cross-section 0.5 x 4.0 mm, with a heater adhered to the back face of the channel with a transparent plexi-glass face for visualisation purposes. Brutin typically uses two identically dimensioned minichannels; one which is used to gather heat transfer data, with thermocouples placed along the flow length of the channel, and another that is used purely for flow visualisation with no thermocouples present. This is a common trend among researchers.

Also in the literature there are many researchers who provide uniform heating to their microchannels, typically via electrical resistance to metal tubing. Kew and Cornwell [3] used as their minichannels, stainless steel circular tubing of inner diameter range 1.39-3.69 mm, heated via d.c. current. Wambsganss et al. [7] used a circular minichannel of inner

diameter 2.92 mm, constructed of stainless steel and heated via d.c. current. Tran et al. [9] used two different geometry minichannels; one circular of inner diameter 2.46 mm and the other rectangular of hydraulic diameter 2.40 mm, both channels were heated by means of electrical resistance and d.c. current. Even though these researchers manage to provide uniform heating to their mini and microchannels, they are not able to visualise the flow inside the channels whilst heating it.

Infrared thermography has been previously used in the literature in determining heat transfer measurements. Hetsroni et al. [32] conducted an experimental study where they coupled an IR camera with high speed imaging for temperature and flow pattern analysis inside mini and microchannels. Temperature profiles generated by evaporative cooling of meniscus interfaces inside capillary tubes have also been investigated with the use of an IR camera by Buffone and Sefiane [33]. The IR technique has also been successfully applied to study boiling [34], mainly due to its fast time response.

The objective of this work is to look in detail at a particular flow instability, under set experimental conditions, using various data; namely IR camera for temperature profiles, pressure sensors measuring the channel pressure drop, and high speed camera imaging the flow. It is possible to measure the local heat transfer coefficient at the same time as recording the local flow visualisation. This data will be analysed and discussed in detail, paying particular attention to the three timescales evidenced in the occurrence of flow instabilities.

2. EXPERIMENTAL APPARATUS

The novel aspect of this research is the simultaneous data acquisition of pressure, temperature, wall heat transfer parameters and flow visualisation. This has been made possible due to a transparent, metallic deposit of Tantalum on the exterior wall of rectangular microchannels of hydraulic diameter 727 μm, and the use of an infra red camera. This tantalum deposit is both conductive and transparent at the thickness sputtered, hence enabling *simultaneous* uniform heating and visualisation of the microchannel flow. The IR camera allows us to measure the local temperature on the microchannel wall, and hence to deduce the heat transfer coefficient along the microchannel whilst simultaneously visualising the fluid flow inside. This, to the best of our knowledge, has not been achievable before due to the intrinsic difficulty of obtaining the heat transfer coefficient, at the same time as visualising the flow.

An experimental apparatus has been designed to induce boiling, to measure parameters across the channel such as temperature and pressure drop and to visualise and record the phenomena occurring inside a microchannel test section. The working fluid chosen is n-pentane, due to its low saturation temperature and hence its low power requirements to induce boiling. The final flow loop consists of an injection system, a test section with a microchannel, a condensation system, a flow visualisation system, and a data acquisition system, all housed inside a temperature regulated box, of volume 1 m^3, see figure 1. The flow loop is regulated at a temperature of 34 °C, (and at atmospheric pressure), just below the saturation temperature of n-pentane which is 35.5 °C.

The injection system uses a glass Luer® lock syringe pump to produce the required constant low liquid mass flowrate through the system. The microchannels in the test section can be interchanged. This is considered so as to demonstrate the influence of the channels dimensions on the flow patterns and heat transfer data achieved. The rectangular

geometries have parallel faces which, once aligned, allow flow visualisation without distortion. The inlet and outlet pressures and temperatures of the microchannel test section can be read and recorded simultaneously via a National Instruments® data acquisition system. The pressure sensors used (Honeywell® 24PC differential series) are accurate to ± 0.25 % span, and the thermocouples used are k-type, and accurate to ± 0.05 °C.

The heating method is electrical resistance via an external metallic deposit, Tantalum (Ta), on the exterior wall of the microchannels. This is novel, since it is allows simultaneous heating and visualisation of the microchannels. The metallic deposit has been sputtered at such a thickness that it is both transparent and conductive, and uniform across and along the microchannel. The resistance of the metallic deposits varies between 3-10 kΩ. The channel is connected to a power supply by means of two thin wires held in place by a conductive silver epoxy, see figure 2. A cold light (Dedolight® 400D) is used providing back lighting, in conjunction with a high-speed camera (Nanosense® MKII, IDT systems) and an interchangeable macro or micro lens as appropriate.

An Infra Red camera (FLIR Systems® ThermaCam SC3000) is used to obtain the temperature profile along the microchannel during the flow boiling experiments. The IR technique is a non-contact, non-destructive test method. Its unobtrusive nature makes it very appealing for temperature determination at the micro scale. The IR camera used here is a multi detector one, with a spatial resolution in the order 10 µm. Other thermal detection techniques, such as unsealed thermochromic liquid crystals (TLCs) have a greater spatial resolution of approx. 1 µm. However, TLCs are time consuming due to their necessary in situ calibration, and also not suitable for our application. This is due to the fact that a layer of black paint is required on the surface to be measured, which would not only interfere with our metallic deposit, but also ruin the visibility of our transparent microchannels for flow visualisation. Another positive feature of IR cameras with photon detectors is their quick time response, in the order of micro seconds, since radiation travels

at the speed of light. The camera has a thermal sensitivity of 20 mK at 30 °C, an accuracy of 1% or 1 °C for temperatures up to 150 °C, a resolution of 320 x 240 pixels, and is Stirling cooled to 70 K. The system provides for automatic transmission correction of temperature, based on the atmospheric temperature, relative humidity, and input distance from the object. The frame rate of the system is up to 50 Hz. The IR camera was used with a microscope lens and a dedicated PC for acquisition, with specialised software (Thermacam Researcher Professional®) for image analysis. The emissivity of the microchannel and its deposit is calculated using a function contained within the Thermacam software. All our rectangular microchannels are fabricated from borosilicate glass, which is an opaque material to IR radiation.

The IR camera detects the temperature profile at the exterior wall of the microchannel, and not the temperature profile of the fluid inside the microchannel. It is hence important to make a calculation of the diffusion time, i.e. the time taken for the temperature at the inner wall touching the fluid, to reach the external wall of the microchannel. Assuming that the thickness of the metal deposit (nanometres) is negligible, and the thickness of the borosilicate glass is in the order of micrometers. An estimate of the diffusion time can be quickly calculated from the thickness of the wall squared, divided by the thermal diffusivity of the wall. A diffusion time of approximately 0.2 seconds is calculated, which is relatively small in front of the flow characteristic time (transit time in the microchannel). The mean transit time of the liquid in the microchannel is 7.83 seconds, based on the mass flowrate through the channel and the channel length. Calculation of the Biot number (Bi), which relates the heat transfer resistance inside and at the surface of a heated body, will allow us to better understand the heat transfer occurring. Comparing the conduction resistance to the convection resistance, a Biot number of 0.02 was calculated. Since $Bi \ll 0.1$, it can be said that the heat conduction inside the body is much faster than the heat conduction away from its surface, and temperature gradients are negligible inside of it. From this, we can state

that the exterior wall temperature field is approximately the temperature field of the interior wall of the microchannel.

3. EXPERIMENTAL PROCEDURE

The n-pentane liquid is degassed to remove non-condensables before it enters the flow loop. The inlet liquid mass flowrate is held constant by the syringe pump during an experimental run. It is also possible to apply a range of heat flux to the test section via electrical resistance, and the power regulator that is connected to the microchannel. Bubble nucleation, expansion and coalescence, slug flow, plug flow, dry-out and other instability phenomena can be observed in the test section with the use of a high-speed camera and macro lens. Observations of a liquid-vapour interface, its progression, and subsequent evaporation of the thin liquid film are recorded through the test section.

Pressure and temperature readings at the inlet and outlet of the channel, IR temperature profiles at the exterior of the microchannel wall, in conjunction with flow visualisation images obtained, have provided simultaneous data showing flow reversal and other flow instabilities.

4. RESULTS

Presented in the following sections are results highlighting the flow instabilities, in terms of pressure, temperature and heat transfer coefficient data, and high speed flow images. The conditions of the case chosen are: rectangular microchannel of hydraulic diameter 727 μm, cross-section 0.4 x 4.0 mm, heated channel length 0.08 m, uniform heat flux (Q) applied to the microchannel was 4.26 kW/m^2 and inlet liquid mass flowrate (m) was held constant at 1.13x10^{-5} kg/s (injection speed of inlet liquid= 1.15x10^{-2} m/s).

Several interesting features are noted during the high speed flow images; the evaporation of the thin liquid film, droplets entrained in this film, slug flow, bubble nucleation, dry-out, 'vapour explosions' and the exiting liquid falling back down into the vapour.

Flow instabilities during two-phase flow boiling are recorded in the microchannel test section, producing peaks in the pressure and temperature signals, see figures 3-5. The pressure drop (ΔP) is simply the difference between the inlet and outlet pressure across the microchannel, and is measured in mbar. The average temperature (T_{avg}) is the average temperature of one heated face (larger cross-section of 80 x 0.04 mm) of the microchannel calculated using *Thermacam Researcher Professional* software, and is measured in degrees Celsius (deg C). The average heat transfer coefficient (h_{avg}) is measured in W/m^2.K, and is calculated directly from the IR temperature data, using the equation shown:

$h_{avg} = \frac{Q}{T_{avg} - T_{sat}}$, where Q is the heat flux measured in W/m^2, and T_{sat} is the saturation temperature of the working fluid in deg C.

An infra red profile of the temperature at the exterior wall of the microchannel illustrated as both a 3D and a contour plot, can be seen in figures 3a and 3b, showing the microchannel during a uniform heating, with applied heat flux 4.26 kW/m^2, over a time period of 80 seconds. In figure 3a, it is evident along the time axis that there are periodic fluctuations in the temperature profile, these are also evident in the 2D graphs of figure 5, where they are observed in more detail. It is interesting to note the periodic oscillations of temperature are at similar amplitude approx. 16 °C, culminating in one larger peak of amplitude approx. 35 °C. The initial, smaller oscillations are due to vapour slugs entering and filling the channel cross section before exiting the microchannel. The larger peak represents an instance of channel dry-out, caused by entire evaporation of the thin liquid

film at that instant. These flow observations were enabled from analysing the corresponding high-speed movies recorded.

The temperature fluctuations on the outside wall of the microchannel, as recorded by the IR camera above, are correlated to the passage of vapour bubbles and slugs inside the microchannel, see figures 4-6. It is important here to point out that there are three timescales involved in the analysis of these pressure and temperature data: there is data as expressed in figure 4 over a time period of 100's of seconds, data as illustrated in figure 5 over a time period of 10's of seconds, and data as illustrated in figure 6 over a time period of several seconds.

The experimental conditions for figures 3-9 are: microchannel heat flux=4.26 kW/m^2, constant inlet liquid mass flowrate= 1.13x10^{-5} kg/s and microchannel hydraulic diameter= 727 μm , which implies for all cases that the flow has already passed the onset of boiling condition for the hydraulic diameter microchannel given, based on previous data obtained. In figures 4-6 shown, the pressure and temperatures fluctuations are those during periodic boiling.

In figure 4, data over a time period of 750 seconds is presented. Large temporal fluctuations can be seen in both the temperature data and the pressure data. These peaks in the temperature and pressure data are well correlated over the whole time period. It can be seen in the temperature data of fig. 4, that there exists both larger amplitude fluctuations (approx. 35 °C and 25 °C) with long periods (approx. 300 and 150 seconds), and also smaller amplitude fluctuations (approx. 16 °C) with a short period (approx. 15 seconds).

During the temperature and pressure data collection process, the boiling phenomena are captured simultaneously by a high speed camera. From analysis of the video images (see figure 7), these small-amplitude/short-period fluctuations appeared to have been caused by the bubble dynamic instabilities during the two-phase flow period. This finding is very similar to that noted by Wu and Cheng [35], who also presented correlated temperature and

pressure data. In addition to this behaviour observed in our experiments; fluctuations at shorter timeframes were revealed, see figure 7. Thanks to the high sensitivity of our pressure and temperature measurements, we could pick out fluctuations at much smaller timescales.

In figure 5, data over a time period of 80 seconds is presented. Again the various peaks in both the temperature, average heat transfer coefficient and the pressure data are well correlated. There are periodic fluctuations in both the temperature, heat transfer and pressure data, of approx. frequency 0.067 Hz, with the magnitude of the temperature fluctuations being approx. 16 °C and the magnitude of the pressure fluctuations approx. 25 mbar. The pressure fluctuations occur just after the peak of the temperature fluctuation has been reached. The pressure continues to fluctuate during the negative gradient region of temperature peak. The pressure has a more constant increasing tendency (from 5-10 mbar) during the positive gradient region of the temperature peak.

As intrinsically expected, the average heat transfer coefficient is at its maxima during the minima of the average temperature fluctuations, and vice versa. The maximum fluctuation in the average heat transfer coefficient was approx. 1000 $W/m^2.K$ at time t=33 s, with average fluctuations at around 500-700 $W/m^2.K$.

It is interesting to note here that the pressure is positive during the first four re-occurring peaks of frequency 0.067 Hz (in the time period of 0-58 seconds). The following peak, that starts to occur at time t=58 seconds has an inflection at time t=66 seconds with T_{avg}=54 °C, which follows the cyclic pattern of the first four peaks. However this peak is just an inflection point, and the actual peak continues to increase to reach a maxima at time t=80 seconds of T_{avg}= 77 °C. The corresponding fluctuations of pressure produce a negative pressure drop across the microchannel of approx. -14 mbar which increases to +22.5 mbar over a time period of acquisition of 7.5 ms. This is indeed a fast phenomenon.

The data shown in figure 6 demonstrates that during a flow instability where periodic pressure and temperature data can be correlated, there are also instabilities occurring at the microscale too. A pressure fluctuation of magnitude 16 mbar occurs during a temperature fluctuation of approx. 0.9 °C at time t= 16.8 seconds, where the corresponding fluctuation in the average heat transfer coefficient is approx. 50 $W/m^2.K$. The same occurs again at time t= 18.0 s, where a temperature fluctuation of approx. 0.8 °C results in a pressure fluctuation of approx. 11 mbar, and a fluctuation in the average heat transfer coefficient of approx. 70 $W/m^2.K$. (Although it is important to mention here that these temperature fluctuations of 0.8 and 0.9 °C are within the range of uncertainty of the IR camera).

As previously discussed, there are phenomena occurring at three different timescales. The data presented in figure 7, shows images taken with a high speed camera at a relatively low frame rate of 200 fps. This was done so as to observe the phenomena occurring over 100's of seconds timeframe.

A vapour slug fills the microchannel. The liquid-vapour interface of this slug begins to pertubate, and deform. This perturbation of the interface grows over time. This produces a bubble to be generated in the bulk fluid. Interpreting this observation further, the mechanisms of vapour evaporation must be looked at in more detail. Vapour recoil could be the dominant effect here. As molecules are leaving the vapour phase, they exert a recoil force on the liquid phase, hence prompting reverse flow and thermocapillary instabilities. During strong evaporation it can be seen that the interface deforms, this also appears to be a cyclic phenomenon, occurring over a time period of approximately 38 seconds. This breakdown of the liquid-vapour interface can be seen in more detail in figure 8, where the frame rate of the high speed camera was 2500 fps.

Figure 8 demonstrates very clearly, that the deformation of the liquid-vapour interface is a very fast phenomenon. Over a time period of 0.4 ms, the meniscus has interacted with the microchannel wall, and begun to deform at the edge. This deformation has an almost ripple effect across the whole interface. The deformation that initially appeared at the right-hand wall, has now progressed as far as the centre of the meniscus, and is much more defined. The high speed video recorded also allows the buoyancy effect of the meniscus in the microchannel to be seen. This particular flow instability settles down after a time period of approximately 40 ms, and is also a cyclic phenomenon.

Initially in figure 8, there is de-wetting at the edge of the microchannel, first occurring at t=0.4 ms. Over a time period of 0.4 ms we can clearly see that the meniscus starts to become de-stabilised, and de-wetting at the wall is observed. This instability propagates across the interface; a likely mechanism for this is vapour recoil, due to intense evaporation at the microchannel walls and the de-wetting phenomenon. The onset of this interface oscillation led to a corresponding overpressure in the microchannel.

The images seen in figure 9 were taken with a high speed camera at a frame rate of 1000 fps. Instability of the thin liquid film at the microchannel wall can be visualised here. It is also a cyclic phenomena, re-occurring over 12 frames (time period= 12 ms). The high curvature at the edges of the microchannel, due to the nature of the geometry, leads to strong capillary effects, where the liquid is sucked towards the channel edges. This liquid film becomes unstable due to the high wall temperatures and high evaporation rates present in the microchannel.

All the flow imaging data presented has added another depth to aid in understanding the phenomena occurring inside the microchannel at equivalent instances to the global data across the microchannel, such as average temperature, average heat transfer coefficient and pressure drop. The flow and interface instabilities described in figures 8 and 9 are clearly correlated to pressure and temperature fluctuations. This corroborates the idea that various

mechanisms operating at different timescales are present during flow boiling in a microchannel.

5. CONCLUSION

Understanding two phase flow boiling in microchannels is of paramount importance to many applications. Many gaps in microchannel research and knowledge are still challenging boiling researchers, particularly in the area of flow instabilities.

Several types of flow reversal and instabilities are observed experimentally in rectangular microchannels (here presented d_h= 727 μm). The novel aspect of this work is the simultaneous measurement of the local heat transfer coefficient in conjunction with local flow visualisation, and pressure drop measurements across the microchannel. This was achieved through the use of a sensitive infrared camera, and a novel, transparent, conductive metallic deposit on the exterior of the microchannels. The flow instabilities are captured both in terms of temperature and pressure fluctuations, as well as visually with a high speed camera. Vapour recoil instabilities are believed to be responsible for triggering flow reversal and high fluctuations in both temperature and pressure. High speed imaging gave evidence for flow reversal and liquid-vapour interface instability.

It was possible to correlate the temperature and heat transfer coefficient data to the pressure data collected, during experimental runs. Phenomena over three timescales could be noted.

ACKNOWLEDGMENTS

The authors would like to thank the Engineering and Physical Sciences Research Council (EPSRC) for their support through a DTA grant.

NOMENCLATURE

Symbol	Description	Unit
Bi	Biot number	
d_h	hydraulic diameter	m
h	heat transfer coefficient	$W/m^2.K$
L	channel length	m
m	liquid mass flowrate	kg/s
P	pressure	Pa
Q	Heat flux	W/m^2
t	time period	s
T	temperature	°C

Greek

ΔP	Pressure drop ($\Delta P = P_{in} - P_{out}$)	Pa

Subscripts

avg	average
in	inlet conditions
out	outlet conditions
sat	saturation

REFERENCES

1. Tuckerman, D.B. and R.F.W. Pease, *High-performance heat sinking for VLSI.* 1981. ED-2(5): p. 126-129.
2. Lin, S., K. Sefiane, and J.R.E. Christy. *Prospects of confined flow boiling in thermal management of microsystems*. 2002. Nottingham, UK: Elsevier.
3. Kew, P.A. and K. Cornwell, *Correlations for the prediction of boiling heat transfer in small-diameter channels.* Applied Thermal Engineering, 1997. 17(8-10): p. 705-715.
4. Carey, V.P., *Liquid-Vapour Phase-change Phenomena.* Hemisphere Publishing Corporation, New York, 1992.
5. Peng, X.F. and B.-X. Wang, *Forced convection and flow boiling heat transfer for liquid flowing through microchannels.* International Journal of Heat and Mass Transfer, 1993. 36(14): p. 3421-3427.
6. Kandlikar, S.G., *Fundamental issues related to flow boiling in minichannels and microchannels.* Experimental Thermal and Fluid Science, 2002. 26(2-4): p. 389-407.
7. Wambsganss, M.W., et al., *Boiling heat transfer in a horizontal small-diameter tube.* Journal of Heat Transfer, Transactions ASME, 1993. 115(4): p. 963-972.
8. Hetsroni, G., et al., *Fluid flow in micro-channels.* International Journal of Heat and Mass Transfer, 2005. 48(10): p. 1982-1998.
9. Tran, T.N., M.W. Wambsganss, and D.M. France, *Small circular- and rectangular-channel boiling with two refrigerants.* International Journal of Multiphase Flow, 1996. 22(3): p. 485-498.
10. Jacobi, A.M. and J.R. Thome, *Heat transfer model for evaporation of elongated bubble flows in microchannels.* Journal of Heat Transfer, 2002. 124(6): p. 1131-1136.
11. Thome, J.R., *Boiling in microchannels: A review of experiment and theory.* International Journal of Heat and Fluid Flow, 2004. 25(2): p. 128-139.
12. Kandlikar, S.G. and W.J. Grande, *Evolution of microchannel flow passages-thermohydraulic performance and fabrication technology.* Heat Transfer Engineering, 2003. 24(1): p. 3-17.
13. Bergles, A.E., et al., *Boiling and Evaporation in Small Diameter Channels. Heat Transfer Engineering,*
Microchannels-Short History and Bright Future, 2003. 24(1): p. 18-40.
14. Moosman, S. and G.M. Homsy, *Evaporating menisci of wetting fluids.* Journal of Colloid and Interface Science, 1980. 73(1): p. 212-223.
15. Dussan V. , E.B. *Moving contact line.* in *Waves on Fluid Interfaces, Proceedings of a Symposium.* 1983. Madison, WI, USA: Academic Press Inc, New York, NY, USA.
16. Renk, F., P.C.J. Wayner, and G.M. Homsy, *On the transition between a wetting film and a capillary meniscus.* Journal of Colloid and Interface Science, 1978. 67(3): p. 408-414.
17. Ajaev, V.S., G.M. Homsy, and S.J.S. Morris, *Dynamic Response of Geometrically Constrained Vapor Bubbles. Journal of Colloid and Interface Science*, 2002. 254(2): p. 346-354.
18. Brutin, D., F. Topin, and L. Tadrist, *Experimental Study of Unsteady Convective Boiling in Heated Minichannels. International Journal of Heat and Mass Transfer*, 2003. 46(16): p. 2957-2965.
19. Hetsroni, G., L.P. Yarin, and E. Pogrebnyak, *Onset of flow instability in a heated capillary tube.* International Journal of Multiphase Flow, 2004. 30(12): p. 1421-1449.
20. Ledinegg, M., *Instability flow during natural forced circulation.* Warme, 1938. 61(8): p. 891-898.
21. Kandlikar, S.G., et al. *High-speed photographic observation of flow boiling of water in parallel mini-channels*. in *2001 National Heat Transfer Conference (NHTC2001), Jun 10-12 2001*. 2001. Ananheim, CA, United States: American Society of Mechanical Engineers.
22. Palmer, H.J., *The hydrodynamic stability of rapidly evaporating liquids at reduced pressure.* Journal of Fluid Mechanics, 1976. 75: p. 487-511.
23. Bose, A. and H.J. Palmer, *Interfacial Stability of Binary Mixtures Evaporating at Reduced Pressure. Journal of Fluid Mechanics*, 1983. 126: p. 491-506.
24. Sefiane, K., D. Benielli, and A. Steinchen, *New mechanism for pool boiling crisis, recoil instability and contact angle influence.* Colloids and Surfaces A: Physicochemical and Engineering Aspects, 1998. 142(2-3): p. 361-373.
25. Hickman, K., *Surface Behaviour in the Pot Still.* Indust. Engng Chem., 1952. 44(8): p. 1892-1902.
26. Xu, J., et al., *Microscale boiling heat transfer in a micro-timescale at high heat fluxes.* Journal of Micromechanics and Microengineering, 2005. 15(2): p. 362-376.

27. Zhang, L., et al., *Phase change phenomena in silicon microchannels.* International Journal of Heat and Mass Transfer, 2005. 48(8): p. 1572-1582.

28. Piasecka, M., S. Hozejowska, and M.E. Poniewski, *Experimental evaluation of flow boiling incipience of subcooled fluid in a narrow channel.* International Journal of Heat and Fluid Flow, 2004. 25(2): p. 159-172.

29. Qu, W. and I. Mudawar, *Flow boiling heat transfer in two-phase micro-channel heat sinks-I. Experimental investigation and assessment of correlation methods.* International Journal of Heat and Mass Transfer, 2003. 46(15): p. 2755-2771.

30. Kenning, D.B.R., Y. Yan, and D.S. Wen, *Saturated flow boiling of water in a narrow channel: time-averaged heat transfer coefficients and correlations.* Applied Thermal Engineering, 2004. 24: p. 1207-1223.

31. Brutin, D. and L. Tadrist, *Pressure Drop and Heat Transfer Analysis of Flow Boiling in a Minichannel: Influence of the Inlet Condition on Two-Phase Flow Stability. International Journal of Heat and Mass Transfer*, 2004. 47(10-11): p. 2365-2377.

32. Hetsroni, G., et al., *Two-Phase Flow Patterns in Parallel Microchannels. International Journal of Multiphase Flow*, 2003. 29(3): p. 341-360.

33. Buffone, C. and K. Sefiane, *IR measurements of Interfacial Temperature During Phase Change in a Confined Environment. Experimental Thermal and Fluid Science*, 2004. 29(1): p. 65-74.

34. Theofanous, T.G., et al., *The boiling crisis phenomenon part I: Nucleation and nucleate boiling heat transfer.* Experimental Thermal and Fluid Science
4th International Congress on Multiphase Flow, 2002. 26(6-7): p. 775-792.

35. Wu, H.Y. and P. Cheng, *Visualization and measurements of periodic boiling in silicon microchannels.* International Journal of Heat and Mass Transfer, 2003. 46(14): p. 2603-14.

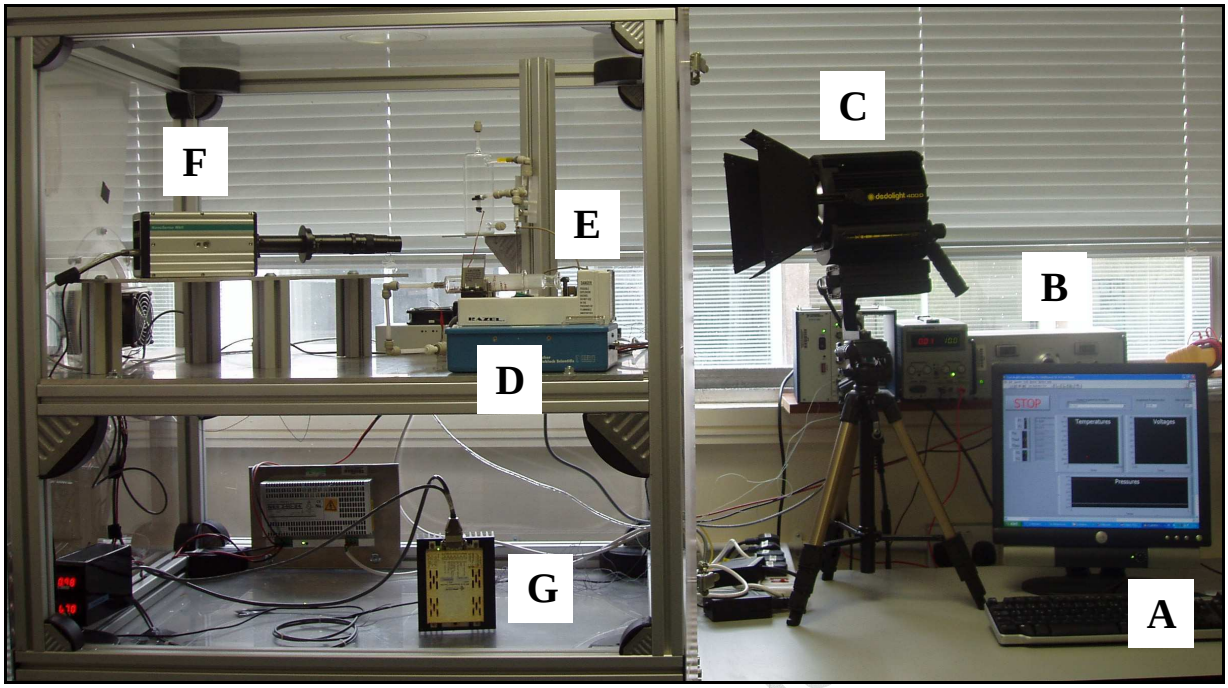

Figure 1: Experimental set-up with back lighting; **A)** Computer data acquisition system, **B)** Power Regulator for microchannel, **C)** Cold light (Dedolight® 400D), **D)** Syringe pump (Fisher Bioblock Scientific®), **E)** Microchannel test section, **F)** Highspeed camera (Nanosense® MKII, IDT systems) and **G)** Heat regulation system.

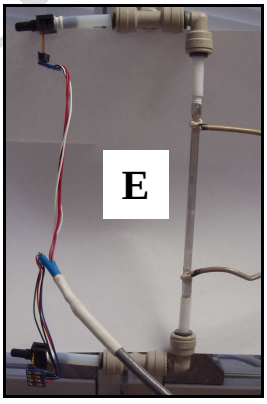

Figure 2: Microchannel test section with pressure (Honeywell® 24PC differential series) and temperature sensors at the inlet and outlet of the microchannel, and wires connected via silver epoxy across the microchannel.

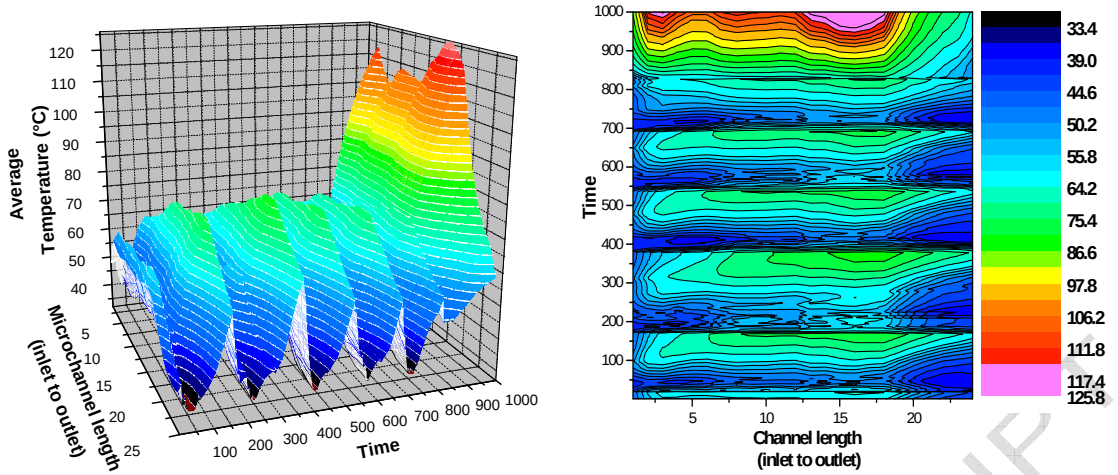

Figures 3a and 3b: 3D plot and contour plot, respectively, showing an IR temperature profile at the exterior of the microchannel during a flow instability. Experimental conditions: uniform heat flux applied to the microchannel= 4.26 kW/m^2, constant inlet liquid mass flowrate= 1.13x10^{-5} kg/s, time period: 1 time unit= 0.08 s (total time= 80 s), and heated microchannel length is (from left to right) the inlet of the microchannel to the outlet, where 1 length unit= 3.33 mm (total heated channel length = 0.08 m). The temperature scale (deg C) is shown at the right-hand side of the contour plot.

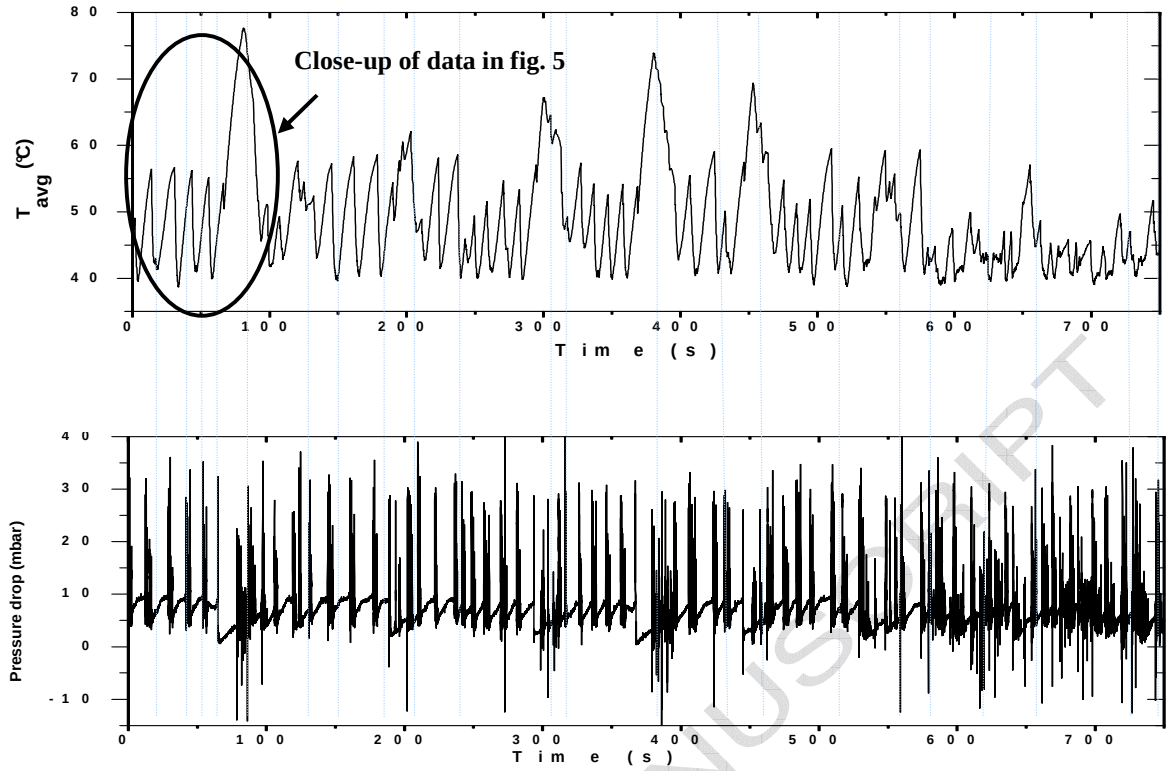

Figure 4: Simultaneous data measurements of average temperature profile and pressure drop across the microchannel. Experimental conditions: uniform heat flux applied to the microchannel= 4.26 kW/m^2, constant inlet liquid mass flowrate= 1.13x10^{-5} kg/s, and time period of 750 seconds.

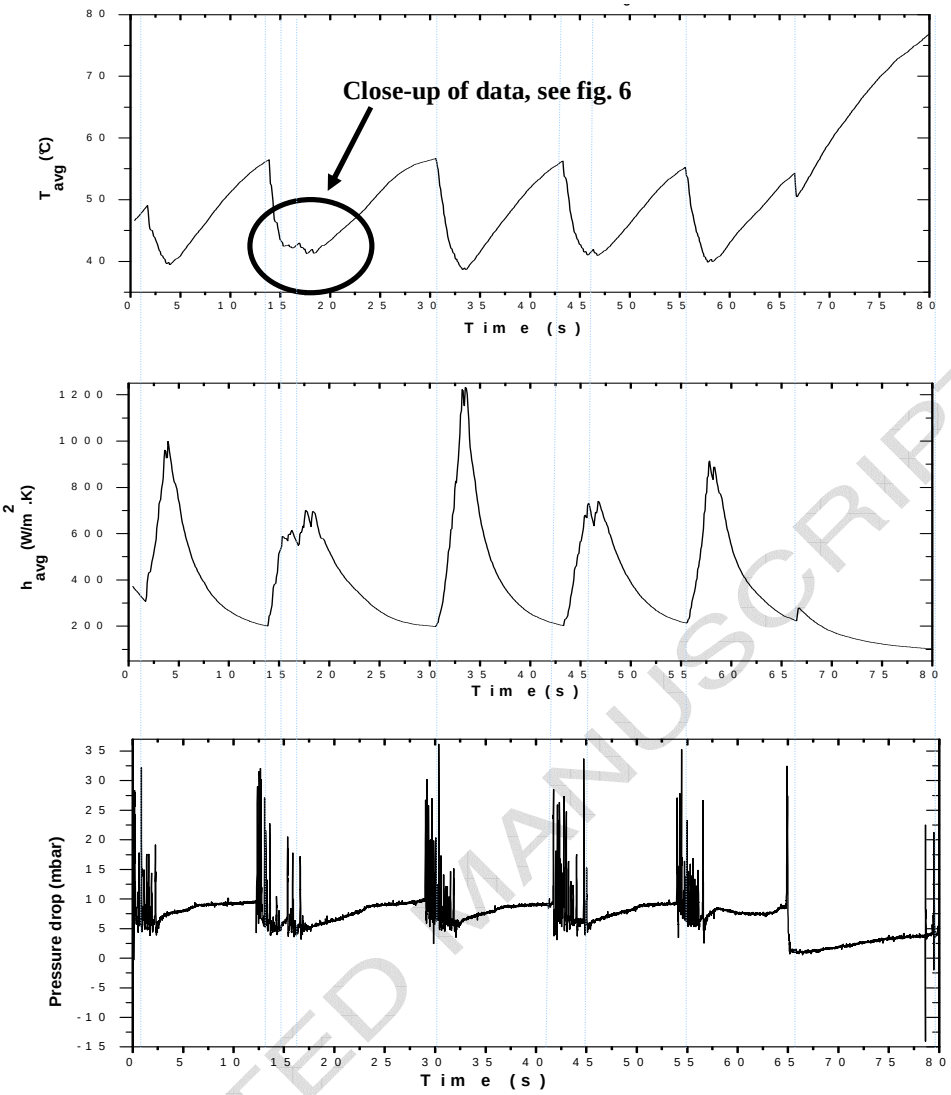

Figure 5: Close-up of simultaneous data measurements of figure 4, looking at a time period of 80 seconds where there are several periodic pressure fluctuations occurring at the same moment as the periodic temperature fluctuations, (same experimental conditions as Fig. 4).

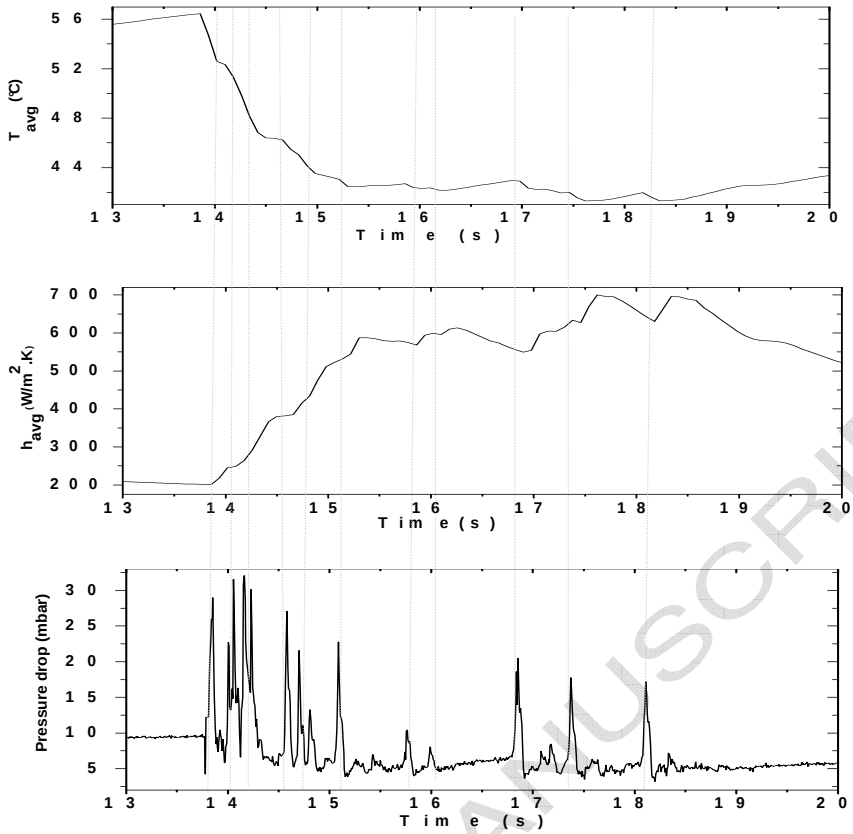

Figure 6: Close-up of simultaneous data measurements of figures 4 and 5, looking at a time period of 7 seconds where there are several simultaneous pressure and temperature fluctuations occurring during an increase in the local heat transfer coefficient, (same experimental conditions as Fig. 4).

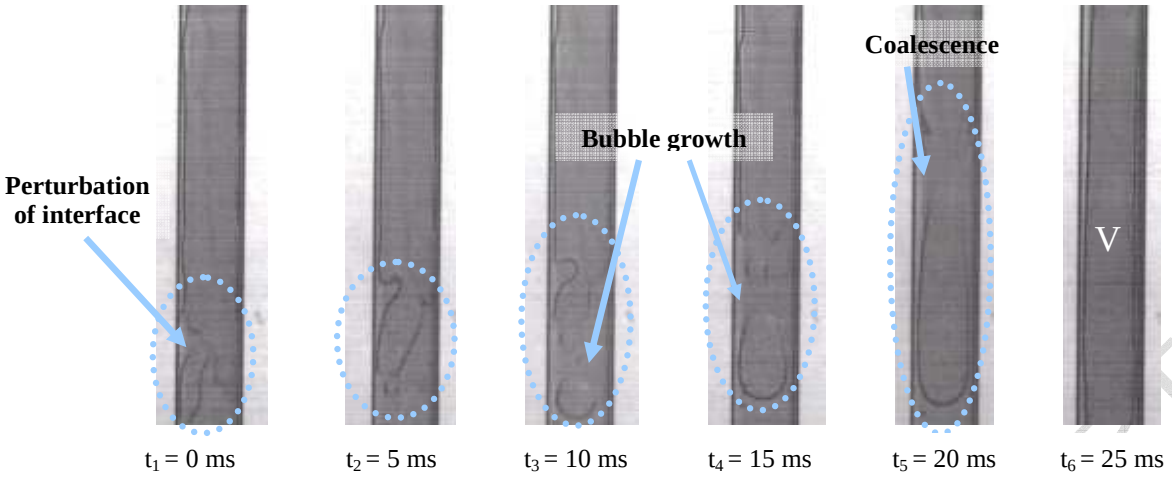

Figure 7: Six consecutive frames illustrating bubble growth and coalescence, leading to a vapour slug filling the channel cross-section within 25 ms, at a camera frame rate of 200 fps, (same experimental conditions as Fig. 4).

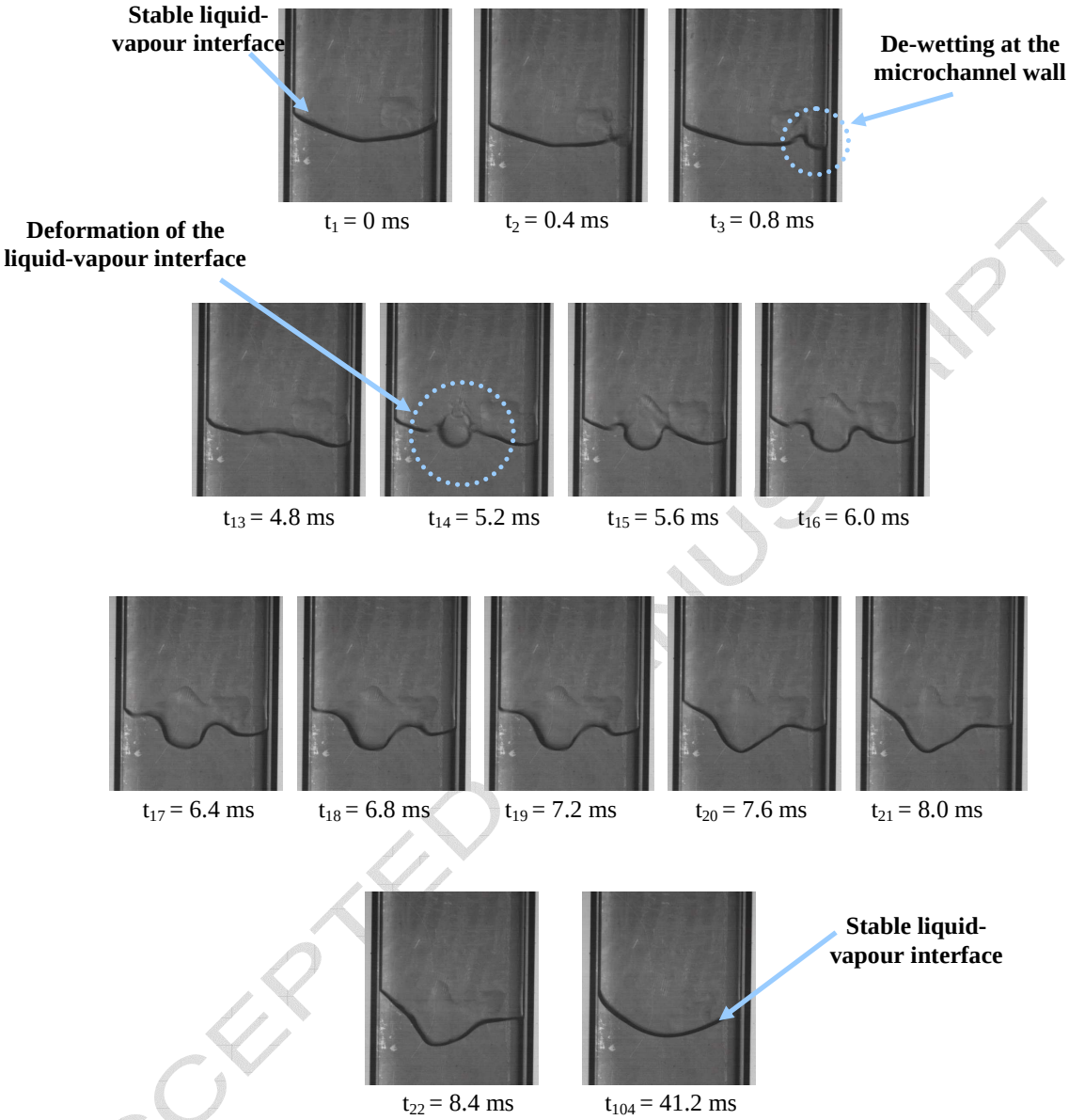

Figure 8: Frames illustrating the breakdown of the liquid-vapour interface during an instability inside the microchannel, at a camera frame rate of 2500fps, (same experimental conditions as Fig. 4).

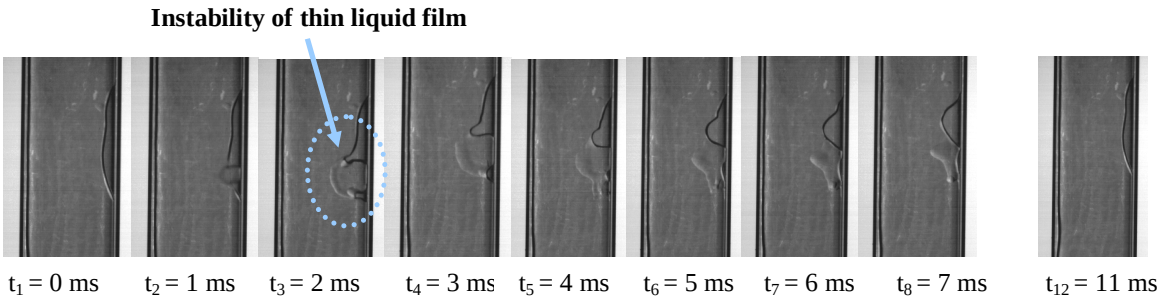

Figure 9: Frames illustrating the instability of the thin liquid film at the microchannel wall, at a camera frame rate of 1000 fps, (same experimental conditions as Fig. 4).